Dielectric relaxations in $Ho_2Ti_2O_7$ and $Dy_2Ti_2O_7$ pyrochlores

Pramod K. Yadav[a], Martin Tolkiehn[b] and Chandan Upadhyay[a*]

[a] School of Materials Science and Technology, Indian Institute of Technology (Banaras Hindu University), Varanasi 221005, India

[b] Deutsches Elektronen-Synchrotron (DESY), Notkestraße 85, 22607 Hamburg, Germany

*Email: cupadhyay.mst@iitbhu.ac.in, Phone: +91-8005304675, Fax: +91-542-2368428

ABSTRACT

Dielectric measurements of $Ho_2Ti_2O_7$ and $Dy_2Ti_2O_7$ cubic pyrochlore show two distinctly defined relaxations around 90K and 36K. The nature and possible origin of these relaxations have been determined. The observed value of critical exponent of Curie-Weiss and Lacroix- *Béné* equation confirms these relaxations are diffuse and show Debye-like behavior. The order of activation energy of $Ho_2Ti_2O_7$ and $Dy_2Ti_2O_7$ shows that both relaxations are distinctly related with structural distortion at oxygen sites. Temperature-dependent lattice volume shows deviation from Debye-Grüneisen behavior below 70 K, further confirms the structural origin of both relaxations. An underlying crystal field anisotropy induced splitting of multipolar order parameter is the primary cause of both diffuse relaxations in these spin ices. It has been found that dielectric relaxations depend strongly on the crystal field, which provides a tool to fine tune the dielectric properties of these systems.

Key Words: Pyrochlore, Spin Ice, Dielectric relaxation, x-ray diffraction

1. Introduction

Geometrically frustrated magnetic rare earth (RE) titanates exhibit a verity of magnetic exotic phases like spin liquid, spin glass, spin ice etc. [1-3]. Lattice geometry plays the major role in these compounds, which leads to magnetic frustration. $Ho_2Ti_2O_7$ (HTO) and $Dy_2Ti_2O_7$ (DTO) spin ices are one of the most studied pyrochlore oxides in which lattice architecture and pronounced crystal field anisotropy decides their geometrical frustrations. This crystal field anisotropy constrains each RE magnetic moment in such a way that it lies along the <111> axis of $Fd\bar{3}m$ crystal structure. Such a spin configuration is termed as classical Ising spin and the Hamiltonian for the crystal field anisotropy can be given as-

$$H_{cf} = -D\sum_i \langle S_i . n_i \rangle^2 \quad (1)$$

where n_i is a unit vector along the Ising <111> axis of the i^{th} spin S_i and D is the anisotropy coefficient [2, 4-7]. These locally constrained Ising spins form a local 2in-2out spin structure. Such configuration of spins has been well-modeled using dipolar and exchange interactions [3,8]. As this spin structure mimic hydrogen ion arrangement in water ice, it gets termed as spin ice structure.

Recently, observation of ferroelectricity in these systems has renewed interests in their theoretical and experimental studies [9-11]. Experimental finding suggests that HTO and DTO, spin ices have multiple ferroelectric transitions of different origin [12]. In polycrystalline HTO two ferroelectric transitions are observed at 60K and 23K [9]. However, in single crystal of HTO, only one transition at 28K has been observed [11]. On the other hand, in polycrystalline DTO two ferroelectric transitions at 25K and 13K have been reported [10]. It has been suggested that ferroelectric transitions at 60K (polycrystalline HTO), 28K (single crystalline HTO) and 25K (polycrystalline DTO) have structural origin [13]. Whereas, ferroelectric transitions at 23K (polycrystalline HTO) and 13K (polycrystalline DTO) are related to the magnetism of these system [9,10].

The presence of ferroelectricity necessarily implies symmetry lowering from cubic $Fd\bar{3}m$ structure of HTO and DTO to a non-centrosymmetric space group (tetragonal, trigonal or lower). This symmetry lowering of space group must originate from phenomenon like-coupling of symmetry-breaking macroscopic strains or anomaly in anisotropic thermal parameters across the

transitions etc. However, these compounds have space group ($Fd\bar{3}m$) in which structural order parameter doesn't couple to the gyrotropic order which belongs to the A_{1u} irreducible representation of the O_h point group [14]. This means that in these spin ices magnetism induced dielectric relaxations can be possible without any structural phase transitions. However, factors responsible for these transitions and its associated nature are still unknown and a matter of investigation.

Herein, the nature of dielectric relaxations in HTO and DTO, observed at temperatures above the spin ice transition temperature, using dielectric spectroscopy being presented. It has been found that both HTO and DTO exhibit distinctly separable two prominent dielectric relaxations at ~90K and ~36K. The determined value of critical exponent γ in the modified Curie-Weiss equation confirms that it is a diffuse phase relaxation (DPR). Through the measured value of activation energy (E_a) and dielectric response of chemically induced structural distortions, triggered by Fe substitution at A & B-site, it has been confirmed that both DPRs at 90K and 36K are Debye-like, which gets inherently generated and related to the lattice distortions at oxygen sites. These observations and possible mechanism are now discussed in details.

2. Pyrochlore structure

The crystal structure of both $Ho_2Ti_2O_7$ (HTO) and $Dy_2Ti_2O_7$ (DTO) shows crystallographic symmetries of space group $Fd\bar{3}m$, having Ho/Dy and Ti at 16d and 16c Wycoff positions respectively. These crystallographic sites form a three-dimensional network of corner-sharing tetrahedra, which in turn makes this system a geometrically frustrated lattice. Fig.1 shows a part of the crystal structure of HTO/DTO pyrochlore lattice. In the pyrochlore lattice, the oxygen environment around both cationic sites is quite interesting. The Ti ion is located in octahedral voids of $Fd\bar{3}m$ structure, whereas Ho/Dy ion is surrounded by eight oxygen ions. On the basis of oxygen position around Ho/Dy ion, we can categorize them in two subclasses: the O1 sites (48f-Wycoff position) and O2 sites (8b-Wycoff position). The O1 oxygen is displaced in two parallel planar equilateral triangles arranged in an antiprismatic manner around the central Ho/Dy ion. This antiprismatic arrangement of O1 oxygen having D_{3d} point group symmetry facilitates large distortion from the ideal cubic structure. This oxygen distortion from the ideal cubic structure is defined by the value of x in the 48f site. For pyrochlore oxides x usually lies in the range 0.320 - 0.345, whereas x=0.3125 shows perfect octahedron around the 16c site. The remaining two

oxygen ions termed as O2 are linearly aligned above and below Ho/Dy ion along local <111> axis of $Fd\bar{3}m$ space group. The distance between Ho/Dy and O2 is ~2.2 Å. This distance between Ho/Dy and O2 is the shortest one known for any rare earth ions, which produces a strong single ion anisotropy (SIA) along local <111> axis. This strong SIA is responsible for the Ising nature of Ho/Dy spin [4, 6, 15].

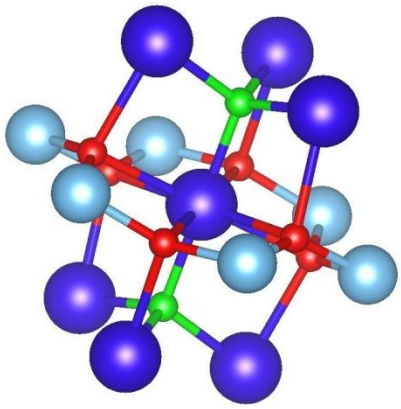

Fig. 1. A part of pyrochlore structure of $R_2Ti_2O_7$ cubic oxides (R = Ho/Dy) highlighting the oxygen environment around Rare Earth ion (blue color) and Ti ion (sky blue color) formed by O1 (red color) and O2 (green color) oxygen sites.

3. Experimental

3.1 Synthesis

Pure phase Polycrystalline sample $Ho_2Ti_2O_7$ (HTO), $Dy_2Ti_2O_7$, (DTO), $Ho_2Ti_{1.85}Fe_{0.15}O_7$ (HTFO), and $Ho_{1.9}Fe_{0.2}Ti_2O_7$ (HFTO) were synthesized by the conventional solid-state reaction methods [16]. To synthesize the samples, stoichiometric proportion of high-purity powder of Ho_2O_3 (≥99.9% assay, Sigma Aldrich), Dy_2O_3 (≥99.9% assay, Alfa Aesar), TiO_2 (≥99.8% assay, Sigma Aldrich) and Fe_2O_3 (≥99.0% assay, Sigma Aldrich) were mixed using an agate mortar. Further, these mixtures were homogenized in acetone medium by mechanical ball milling for 8 h followed by acetone removal at room temperature. Firing of all samples was done at 1350 ^{0}C for 20 h in alumina crucibles. Fired samples were crushed into fine powders using a mortar and pestle. Pellets were made using PVA binder, which was burned by heating the samples at 600 ^{0}C for 12 h. Further, sintering of all samples were done at 1375 ^{0}C for 20 h to obtain the high-density samples.

3.2 X-ray diffraction

$R_2Ti_2O_7$ pyrochlore oxide forms a highly stable structure. In case of $Ho_2Ti_2O_7$ and $Dy_2Ti_2O_7$ and its derivatives, there are no volatile components present. This makes the synthesized compounds as intended. Room-temperature High-Resolution x-ray diffraction (HRXRD) (Rigaku) with Cu $K\alpha_1$ optics near source side was used for phase purity and structural analysis of the samples. For low-temperature structural analysis, synchrotron powder x-ray diffraction (SXRD) data of HTO was collected at beamline P24, PETRA-III, DESY, Hamburg, Germany. The Diffraction pattern was recorded using 25 keV x-ray in 0.7 - 7.3 $Å^{-1}$ Q range. The powder for x-ray diffraction measurements was obtained from crushed sintered pellets, which was annealed at 600 °C for 12 h to remove the stresses introduced during crushing. Rietveld refinement was carried out using the FULLPROF SUITE [17].

The HRXRD pattern of HTO, DTO, HTFO, and HFTO samples and its fitting, in a standard setting with indexing of major peaks, is shown in Fig. 2. For pyrochlore structure having space group $Fd\bar{3}m$, other than the usual profile parameters, variable structural parameters are- lattice constant a, x coordinate of the 48f-site and isotropic thermal parameters. The obtained structural parameters and fitting parameters are listed in table 1. The obtained fit is remarkably good indicating that the samples are defect free and having stoichiometry as intended. However, for Fe-substituted compositions (especially for B-site substituted), charge compensating oxygen deficiency may be generated but its effect is negligible on the crystal structure.

Table 1. Details of structural refinement as obtained from high-resolution x-ray diffraction. Compound, lattice constant, variable coordinate x of the 48f-site, R-factors (R_p, R_{wp} and R_e) and goodness of fit χ^2.

Compound	Lattice constant a (Å)	x value (48f-Wycoff site)	R_p	R_{wp}	R_e	χ^2
$Ho_2Ti_2O_7$	10.1006(1)	0.324(2)	14.8	14.6	6.86	4.55
$Dy_2Ti_2O_7$	10.1270(1)	0.320(2)	21.9	15.4	9.82	2.47
$Ho_2Ti_{1.85}Fe_{0.15}O_7$	10.1013(4)	0.325(1)	14.4	13.5	7.24	3.47
$Ho_{1.8}Fe_{0.2}Ti_2O_7$	10.0804(1)	0.327(1)	21.4	18.1	9.03	4.00

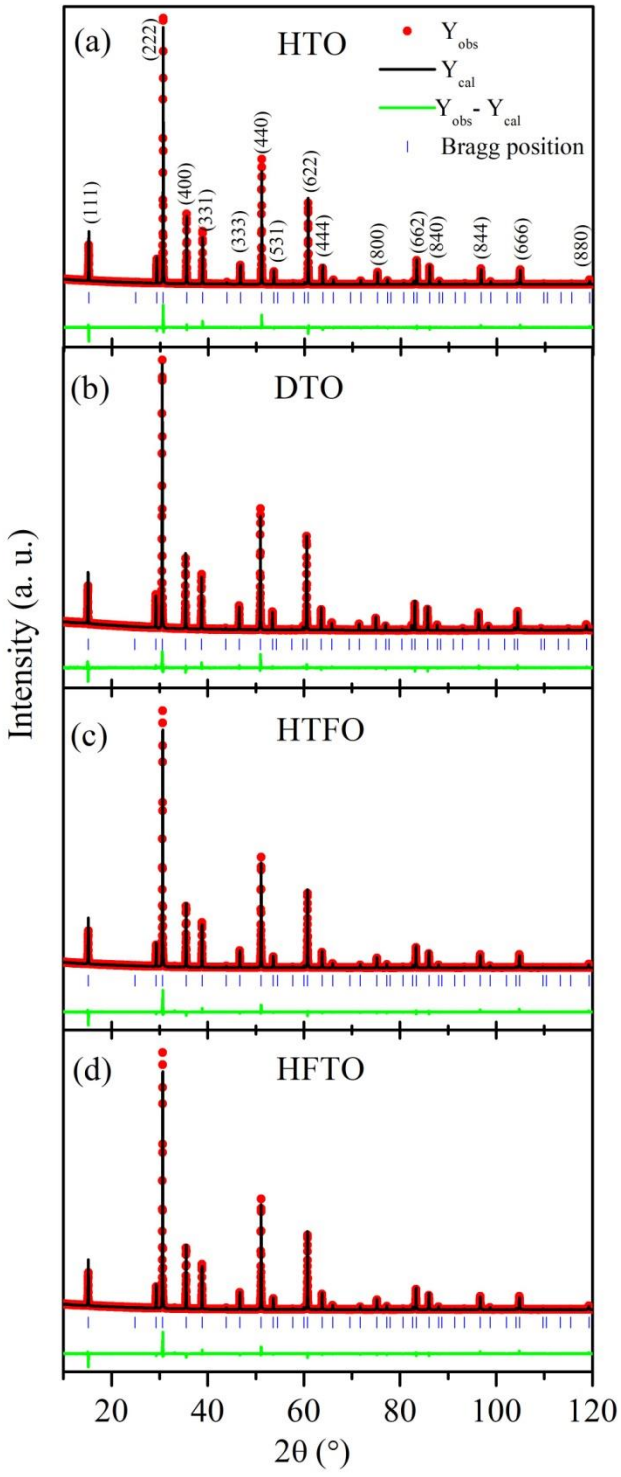

Fig. 2. Rietveld fit of the room temperature High Resolution x-ray Diffraction pattern of polycrystalline (a) $Ho_2Ti_2O_7$; (b) $Dy_2Ti_2O_7$; (c) $Ho_2Ti_{1.85}Fe_{0.15}O_7$ and (d) $Ho_{1.8}Fe_{0.2}Ti_2O_7$.

4. Results and disscussion

Low-temperature dielectric permittivity measurement was performed by using a fully computer-controlled measuring system involving a Novo control Alpha-A high-frequency analyzer and a cryogen-free measurement system. Temperature-dependent dielectric measurement has been performed in a frequency range of 0.5 to 400 kHz for HTO and DTO. The error value in the measurement is less than 0.01%.

Fig. 3 shows the plot of real (ε') and imaginary (ε") part of relative dielectric permittivity vs temperature at different frequencies. It has been found that both HTO and DTO show two successive dielectric relaxations in the temperature range 87-127K and 34-49K respectively. A broad peak develops below ~30K up to lowest measured temperature. At 1 kHz, relaxations are observed at 90K and 36K in case of HTO, while in case of DTO these dielectric relaxations are observed at 92.5K and 37K. The ε" has a tendency to shift with increasing frequency. In this case also ε" show an offset with varying frequency. For HTO; the shift is from 0.025 to 2 as one increases the frequency from 10 kHz and 400 kHz. Similarly, for DTO the offset values change from 0.05 to 2.5 with increasing frequency from 10 kHz and 400 kHz. For 10kHz frequency, the y-scale value for ε" lies between 0.025-0.8 and 0.05-0.5 for HTO and DTO, respectively. It has been found that dielectric relaxation (~90K and ~36K) in HTO and DTO shows large frequency dispersion. The peak temperature $T_{m'}$ for ε' and $T_{m''}$ for ε" shift towards higher temperature side with increasing frequency. This represents a typical feature of diffuse/relaxor nature of the dielectric relaxation. The conclusive way to determine the diffuseness of a dielectric relaxation of the compound, through the obtained value of γ in equation 2 [18]

$$\frac{1}{\varepsilon'} - \frac{1}{\varepsilon'_m} = \frac{(T - T_{m'})^{\gamma}}{C'} \qquad (2)$$

Where, γ and C' are constants. Critical exponent γ is regarded as a measure of the diffuseness of the transition. For normal transitions (Curie-Weiss law) one gets γ=1; for relaxor transitions (for disordered system) one gets γ=2; while 1<γ<2 corresponds to the diffuse transitions. In equation (2) values of ε'_m and $T_{m'}$ are the maxima of the ε' and its corresponding temperature, respectively. To describe the nature of relaxation in HTO as well as in DTO, we determined the critical exponent γ using the above eq. 2. In the plots of $\ln(\frac{1}{\varepsilon'} - \frac{1}{\varepsilon'_m})$ as a function of $\ln(T-T_{m'})$, the slope will give the

value of γ for 90K and 36K relaxation. Fig. 4 (a) and (b) shows the plots of $\ln(\frac{1}{\varepsilon'} - \frac{1}{\varepsilon'_m})$ as a function of $\ln(T-T_{m'})$ for a representative frequency of 1kHz . For HTO, the obtained value of γ is 1.68 and 1.26 for the dielectric relaxation at 90K and 36K respectively. For DTO, the value of γ turns out to be 1.23 for both relaxations, occurring at 92.5K and 37 K. The obtained values of γ for both the compounds thus confirm that both observed dielectric relaxations are diffusive in nature. Diffusive nature of dielectric relaxation is generally associated to the subtle change or rearrangement, of the bonds associated with a particular site of the crystal structure, without breaking lattice symmetries. Unlike other diffuse or relaxor compounds, HTO and DTO do not contain any chemical disorder, both observed diffuse relaxations are likely to be inherently generated by the lattice distortions. In order to investigate the nature of frequency dispersion behavior of both relaxations, ln (τ) vs. $1/T_{m''}$ plot has been fitted by using the Arrhenius equation given as

$$\tau = \boldsymbol{\tau_0} \exp\left(\frac{Ea}{KT}\right) \quad (3)$$

Where τ is the measuring relaxation time in sec, $\boldsymbol{\tau_0}$ is the characteristic relaxation time, and E_a is activation energy given in unit of meV, where τ has been obtained using the relation $\tau = 1/2\pi f$ and f being the applied frequency for the measurement. Figure 4 (c) & (d) show the ln (τ) vs. $1/T_{m''}$ plot with linear fit for both 90 K and 36 K relaxations of both HTO and DTO. The obtained values of E_a and $\boldsymbol{\tau_0}$ for are summarized in Table 2.

Table 2. Value of activation energy E_a (meV) and characteristic relaxation time $\boldsymbol{\tau_0}$ (sec) for 90K and 36K relaxations deduced from-peak position $T_{m''}$ of temperature dependent ε'' and Lacroix-Béné function fitted obtained parameters τ_0 (in the bracket.).

Compound	T_{m1}		T_{m2}	
	E_a (meV)	$\boldsymbol{\tau_0}$ (sec)	E_a (meV)	$\boldsymbol{\tau_0}$ (sec)
$Ho_2Ti_2O_7$	147.2±0.2 (139.8±3)	2.9×10^{-13} (7.0×10^{-13})	56.5±0.2 (50.0±2)	5.5×10^{-13} (3.8×10^{-12})
$Dy_2Ti_2O_7$	155.8±0.2 (138.2±3)	2.1×10^{-13} (1.7×10^{-12})	60.1±0.2 (52.4±1.2)	2.7×10^{-13} (2.4×10^{-12})

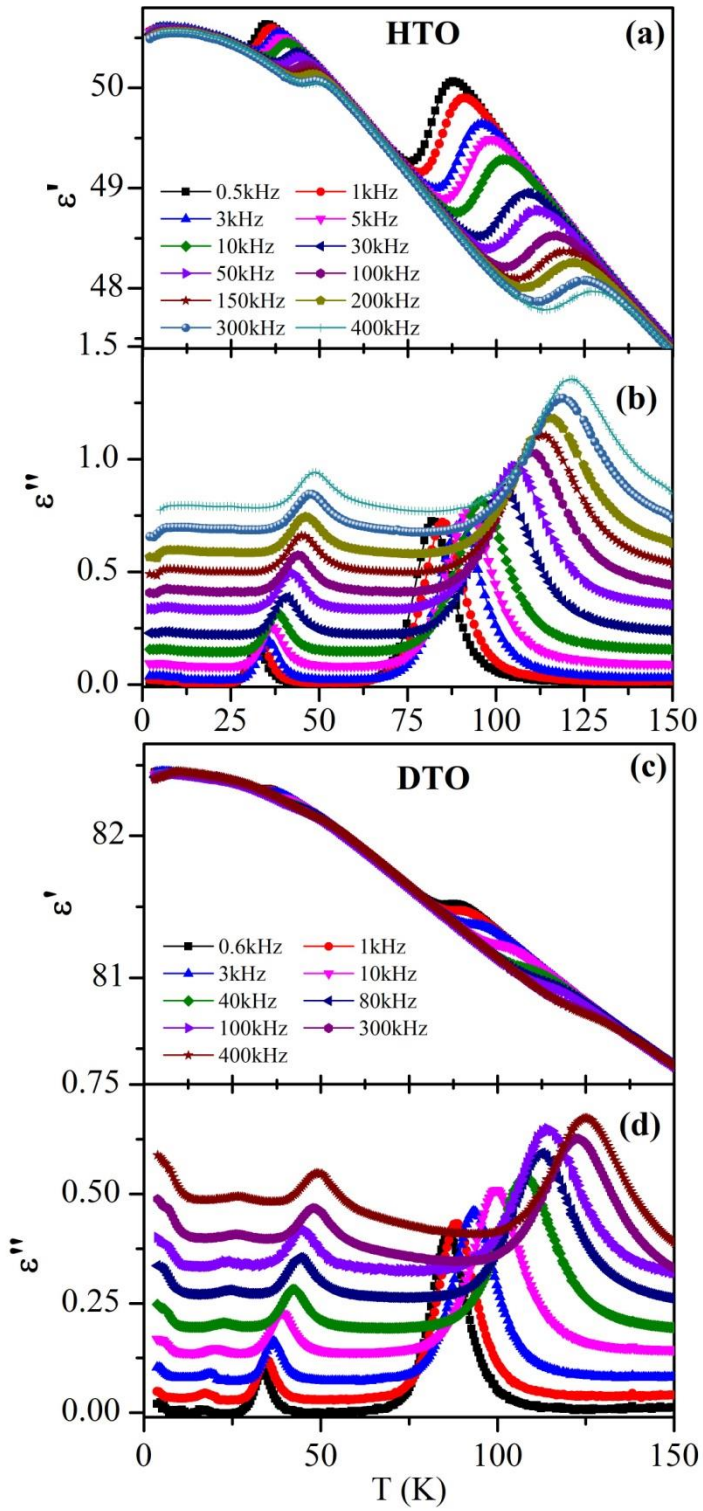

Fig. 3. Temperature dependence of the real (ε') and imaginary (ε'') part of the dielectric permittivity of $Ho_2Ti_2O_7$ (a, b) and $Dy_2Ti_2O_7$ (c, d) measured at different frequencies. The y scale for ε'' belongs to measurement done at 10kHz.

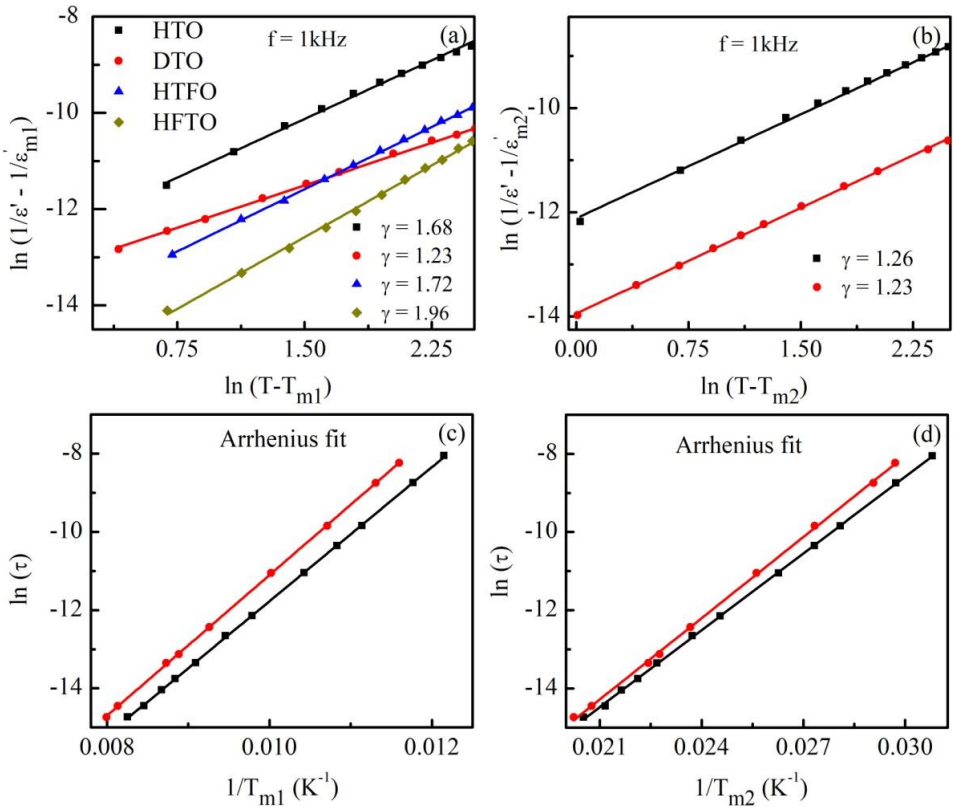

Fig. 4. Plot of (a) ln $(1/\varepsilon'- 1/\varepsilon_{m'})$ as a function of ln $(T-T_{m'})$ at 1 kHz for 90K relaxations for $Ho_2Ti_2O_7$, $Dy_2Ti_2O_7$, $Ho_2Ti_{1.85}Fe_{0.15}O_7$ & $Ho_{1.8}Fe_{0.2}Ti_2O_7$ and (b) 36K relaxations for $Ho_2Ti_2O_7$ & $Dy_2Ti_2O_7$. (c) ln (τ) vs. $1/T_{m''}$ plot with Arrhenius fit for 90K and (d) 36K relaxation observed in $Ho_2Ti_2O_7$ and $Dy_2Ti_2O_7$.

4.1. Lacroix- Béné analysis

Nature of both relaxations of HTO and DTO has been investigated in terms of frequency dependent variation of the dielectric permittivity at fixed temperature. To illustrate the frequency dependence of the dielectric permittivity at fixed temperature we have replotted the Fig. 3. Frequency dependence of the real and imaginary part of dielectric permittivity at different temperature for both HTO and DTO is shown in Fig. S1 of the supplementary text. It has been found that on increasing temperature, both relaxation peak observed in ε" shifted towards the higher frequency side in both compounds. This temperature-dependent variation of the relaxation peak suggests the thermally activated relaxation mechanism. To investigate the nature of relaxation, we fit the ε' vs. f data by using Lacroix- *Béné*-type distribution function of relaxation time, $\tau= 1/2\pi f$ given by [19]

$$G(\ln \tau) = \frac{\sin(\pi\beta)}{\pi} \left(\frac{\tau_0}{\tau - \tau_0}\right)^{\beta} \qquad \text{for } \tau > \tau_0$$

and (4)

$$G(\ln \tau) = 0 \qquad \text{for } \tau < \tau_0$$

The values of τ_0 and β determines the fastest relaxation time and polydispersivity of the system. For monodispersive system one obtained $\beta=1$. In terms of τ_0 and β, the complex dielectric permittivity of polydispersive system becomes

$$\tilde{\varepsilon}(\omega) = \varepsilon_s - (\varepsilon_s - \varepsilon_\infty)\left(1+\frac{1}{i\omega\tau_0}\right)^{-\beta} \quad (5)$$

Where, $\omega= 2\pi f$ and ε_s, ε_∞ are the static and high limit-f of ε', respectively. In terms of ε' and ε'' the expression becomes

$$\varepsilon' = \varepsilon_s - (\varepsilon_s - \varepsilon_\infty)(\cos\lambda)^{\beta}\cos\lambda\beta \quad 6\,(a)$$

$$\varepsilon'' = (\varepsilon_s - \varepsilon_\infty)(\cos\lambda)^{\beta}\sin\lambda\beta \quad 6\,(b)$$

Where, $\lambda= \text{arccot}(\omega\tau_0)$

Table 3. Obtained values of fitting parameters ε_s, ε_∞, β, and τ_0 referring to the dispersion data ε' of figure 5 for $Ho_2Ti_2O_7$ and $Dy_2Ti_2O_7$.

$Ho_2Ti_2O_7$					$Dy_2Ti_2O_7$				
T (K)	ε_s	ε_∞	β	τ_0 (s)	T (K)	ε_s	ε_∞	β	τ_0 (s)
33	50.59(1)	50.28(1)	0.90(1)	1.68×10^{-4}	34	82.34(2)	82.30(2)	0.93(1)	1.48×10^{-4}
35	50.63(1)	50.22(1)	0.88(1)	6.12×10^{-5}	36	82.33(1)	82.27(1)	0.92(4)	5.87×10^{-5}
37	50.60(1)	50.16(0)	0.86(3)	2.46×10^{-5}	38	82.30(1)	82.25(1)	0.92(2)	2.18×10^{-5}
39	50.55(1)	50.12(0)	0.85(1)	1.12×10^{-5}	40	82.28(2)	82.22(1)	0.92(1)	1.03×10^{-6}
85	50.19(3)	48.70(1)	0.95(1)	1.06×10^{-4}	85	81.58(1)	81.43(1)	0.94(1)	2.46×10^{-4}
88	50.10(2)	48.56(2)	0.94(1)	5.66×10^{-5}	88	81.56(1)	81.36(1)	0.93(5)	1.44×10^{-4}
91	50.08(2)	48.41(2)	0.92(1)	3.28×10^{-5}	91	81.51(2)	81.30(3)	0.93(2)	7.94×10^{-5}
94	49.88(2)	48.23(2)	0.89(4)	1.89×10^{-5}	94	81.45(3)	81.24(1)	0.92(4)	4.51×10^{-5}
97	49.73(1)	48.06(2)	0.85(3)	1.07×10^{-5}	97	81.39(1)	81.17(1)	0.92(2)	2.52×10^{-5}
					100	81.33(4)	81.11(1)	0.92(2)	1.49×10^{-5}

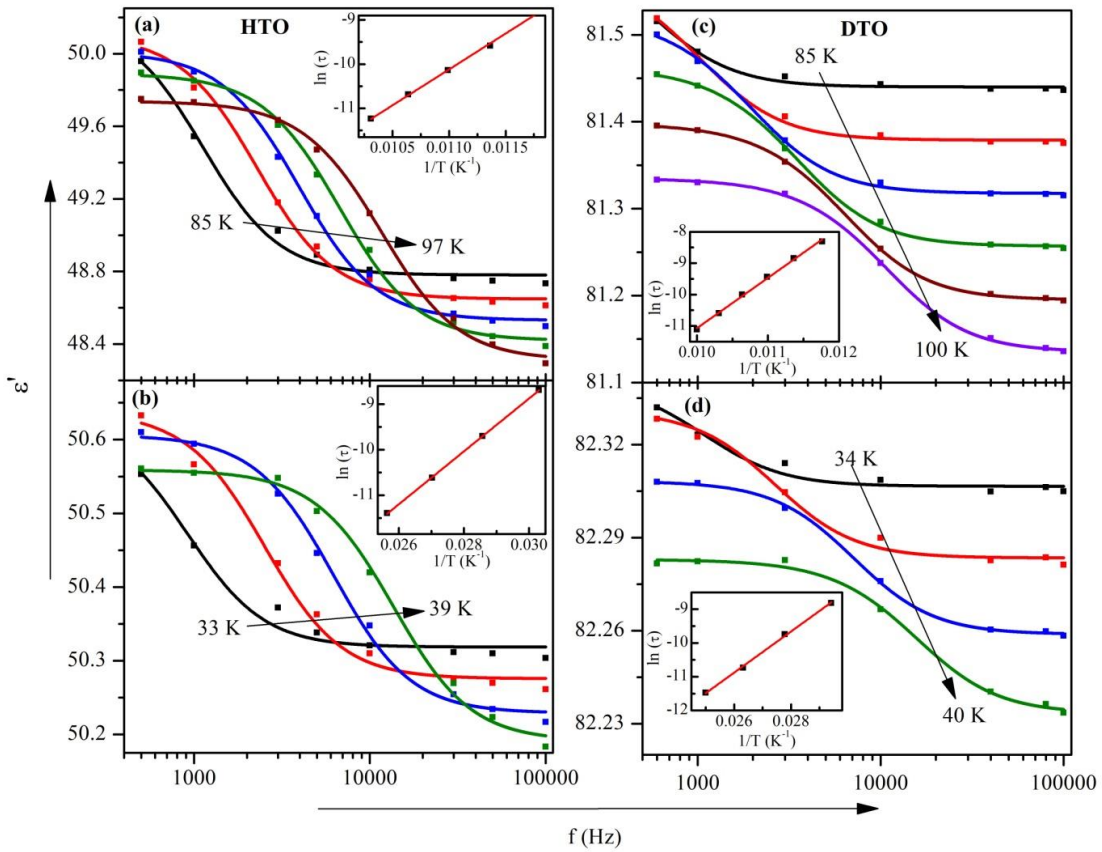

Fig. 5. Lacroix-Béné function fit of ε' vs. f plot at different temperature of $Ho_2Ti_2O_7$ (a, b) and $Dy_2Ti_2O_7$ (c, d). Inset shows the Arrhenius fitted ln (τ_0) vs. 1/T plot.

Figure 5 shows the best fit of ε' vs f plot of both compounds using equation 6 (a) whereas the parameters- ε_s, ε_∞, β and τ_0 obtained from fitting are listed in table 3. The observed values of β for both relaxations lies between 0.85-0.95 ranges (close to 1), suggesting the monodispersive Debye-like nature of relaxations. With the help of obtained values of τ_0, we plot the ln (τ) vs. 1/T to reconfirm the Arrhenius nature and activation energy of both the relaxations observed in HTO and DTO. Inset of Fig. 5 shows the plot of ln (τ) vs. 1/T with linear fit whereas the obtained values of characteristic relaxation time ($\boldsymbol{\tau_0}$) and activation energy (E_a) are listed in table 2 (in the bracket).

The analysis of frequency dependent dielectric permittivity reconfirms that both 90K and 36K relaxation observed in HTO and DTO are thermally activated having similar order of characteristic relaxation time and activation energy as obtained from temperature dependent dielectric permittivity studies. It has been found that the observed value of characteristic relaxation time for both relaxations have same order but different value of activation energy. Relaxation time

originating from polar lattice vibrations lies in the range of 10^{-9}-10^{-14} sec. In case of HTO and DTO, obtained value of τ_0 is in range of 10^{-12}-10^{-13} sec, thus indicating that observed relaxations in HTO and DTO are related to polar lattice vibrational effects because of local distortions. The order of characteristic relaxation time and activation energy as obtained by Arrhenius fit are well correlated with dielectric relaxations observed in $Bi_{1.5}Zn_{1.0}Nb_{1.5}O_7$ and Bi_2O_3–ZnO–Nb_2O_5 cubic pyrochlores [20, 21]. These cubic pyrochlore does not exhibit relaxor phase transition (or freezing typical for relaxors), it exhibits only broad distribution of relaxation frequencies (or times), which broadens on cooling. Nevertheless, the main relaxation time follows the Arrhenius behavior. In these studies, it has been concluded that dielectric relaxation is originated by local distortions in oxygen positions and influenced by phonon branches associated with O1-A-O1 and O2-A-O2 bending modes. In the present study of HTO and DTO, the order of activation energy is ~150meV and ~50meV for 90K and 36K relaxations, respectively. In congruence with the activation energy and assigned phonon modes in ref. 20 & 21, it may be concluded that 90K DPR has originated from local structural distortion in O1 oxygen sites and must be influenced by phonon branches associated with O1-A-O1 bending modes. Accordingly, the 36K dielectric relaxation gets originated by local structural distortion in O2 oxygen site and influenced by the phonon branches associated with O2-A-O2 bending modes. Moreover, if both relaxations are distinctly related to O1 and O2 crystallographic site of the oxygen position then as structure suggests (Fig.1), distortion at B-site should affect only 90K relaxation whereas A-site distortion should affect both relaxations. To further confirm the origin of each relaxation, chemical inhomogeneity at B-site (Ti-site) and A-site (Ho-site) through Fe-substitution has been created and their effects have been studied in detail.

4.2 B-site doped $Ho_2Ti_{1.85}Fe_{0.15}O_7$

Temperature dependence of dielectric permittivity of B-site doped HTFO sample is shown in Fig. 6 (a) & (b). For 10 KHz frequency the y-scale values of ε" lies the range of 0.07-0.25. The offset value for 10 kHz and 300 kHz varied from 0.01 to 2.0. Out of the two relaxations of HTO, only 90 K relaxation is getting affected by this partial substitution. The nature of relaxation has also changed quite significantly. The narrower relaxation present in case of HTO has broadened as well as frequency dispersion smeared out over a wide temperature range. The measured value of γ (at 1 kHz) for HTFO has changed to 1.72 from 1.67 for HTO (Fig.4 (a)). The higher value of

γ shows that the observed phase relaxation is shifting towards a relaxor type but still can be categorized as diffusive in nature.

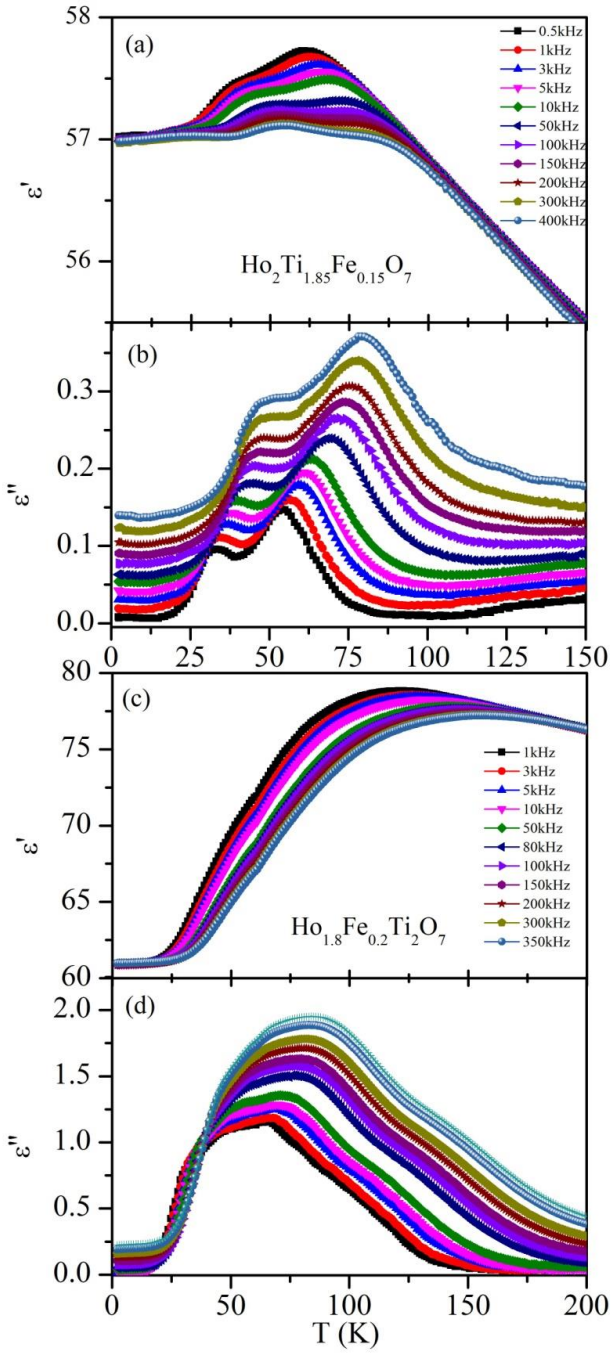

Fig. 6. Temperature dependence of the real (ε') and imaginary (ε'') part of the dielectric permittivity of $Ho_2Ti_{1.85}Fe_{0.15}O_7$ (a, b) and $Ho_{1.8}Fe_{0.2}Ti_2O_7$ (c, d) measured at different frequencies. The y scale for ε'' belongs to measurement done at 10kHz.

4.3 A site doped $Ho_{1.8}Fe_{0.2}Ti_2O_7$

The temperature dependent dielectric permittivity of A-site doped HFTO samples is shown in Fig. 6 (c) & (d). For 10 KHz frequency the y-scale values of ε'' lies the range of 0.01-1.5. The offset value for 10 kHz and 300 kHz varied from 0.01 to 0.2. It is found that A-site Fe doping affects both relaxation temperatures and almost a single relaxation is observed in place of two relaxations in ε' and ε''. The measured value of γ (at 1 kHz) for HFTO turns out to be 1.96 (see Fig. 4a) indicating that this relaxation becomes almost relaxor-like [18, 22].

Table 4. Observed values of bond length and bond angle as obtained from the Rietveld refinement.

Compound	Bond length (Å)			Bond angle (^{0})		
	A-O2	A-O1	B-O1	O2-A-O2	O1-A-O1	O1-B-O1
$Ho_2Ti_2O_7$	2.18684(0)	2.519(3)	1.9361(12)	180(0)	62.88(3)	85.47(12)
$Dy_2Ti_2O_7$	2.19255(0)	2.553(3)	1.9262(15)	180(0)	62.53(4)	86.95(16)
$Ho_2Ti_{1.85}Fe_{0.15}O_7$	2.18700(0)	2.5127(15)	1.9397(8)	180(0)	62.964(19)	85.14(8)
$Ho_{1.8}Fe_{0.2}Ti_2O_7$	2.18246(0)	2.496(3)	1.9421(17)	180(0)	63.12(4)	84.55(15)

The structural data obtained from the Rietveld refinement has been used for calculation of bond angle and bond length between the A/B site with associated oxygens as shown in Fig. 1. Table 4 list the details of these bond lengths and angles. It has been found that for B-site substituted $Ho_2Ti_{1.85}Fe_{0.15}O_7$ (HTFO) sample, only A/B-O1 bond length, and bond angle is getting affected whereas A-O2 bond length and bond angle is nearly unaffected. Contrary to that, for A-site Fe substituted $Ho_{1.8}Fe_{0.2}Ti_2O_7$ (HFTO) sample A/B-O1, as well as A-O2 bond lengths, are affected with a change in O1-A/B-O1 bond angle as well. These results suggest that out of the two diffused dielectric relaxation, prevailing in HTO at 90K and 36K is originating from the distortion in the O1 site and O2 site of the oxygen position respectively. A similar kind of finding has been confirmed by temperature dependent Raman, crystal field excitation and principle elastic constant studies [13, 23-24]. It has been shown that at low temperatures (<120K), a structural distortion in both oxygen position takes place via softening in F_{2g} phonon mode related to O1 and O2 site of oxygen position. In $Fd\bar{3}m$ space group, a gyrotropic order which belongs to A_{1u} irreducible representation of O_h point group is not compatible with any phonon mode related to the structural

order parameters. This clearly indicates that observed transitions can have only an electronic origin [14]. In these RE compounds crystal field anisotropy splits the five-component multipolar order parameter Q_{ij}, into two-dimensional E_u represented as($Q_{xx} - Q_{yy}$, $2Q_{zz} - Q_{xx} - Q_{yy}$) and a three-dimensional T_{2u} represented as (Q_{xy},Q_{yz},Q_{zx}) [25, 26].The splitting of electronic order parameters, which is also responsible for the Ising nature of Ho/Dy spin, are more prominent below 120K [27]. In neutron scattering and nuclear quadrupole resonance (^{47}Ti-NQR) experiments, a monotonic increment in the spin relaxation time has been observed below 120 K [27-29]. Whereas, in temperature dependent crystal field excitations studies, it has been observed that below 130 K various crystal field excitations emerge, which are coupled with the phononic excitations [15, 23, 30-31]. These observations indicate the interconnection between the splitting of multipolar order parameters and structural distortion at the oxygen position.

4.4 Low temperature x-ray diffraction analysis

Furthermore, the splitting of multipolar order parameters and its associated structural distortions are observed below 130 K. This suggests that acting crystal field anisotropy (D) as shown in equation 1 is not simply a constant value, it varies with temperature and becomes more pronounced below 130 K. Due to the coupling of structural order parameters with electronic order parameters, a change in the lattice volume should occur at low temperature in these compounds. Experimental findings suggest that due to the Kramer's nature of Dy ion, in DTO, this effect is more prominent than that of the HTO [13, 32]. To confirm this change in the lattice volume we have performed the low-temperature synchrotron x-ray diffraction (SRXRD) measurement of $Dy_2Ti_2O_7$. Fig. 7 shows the SRXRD pattern of DTO measured at different temperature. In the measured temperature range SRXRD pattern do not shows any structural transition which confirms that at low temperatures DTO pertain its $Fd\bar{3}m$ space group. Fig. 8 shows the part of Rietveld fitted pattern of SRXRD data at different temperature. The details of synchrotron x-ray diffraction analysis are listed in table 5.

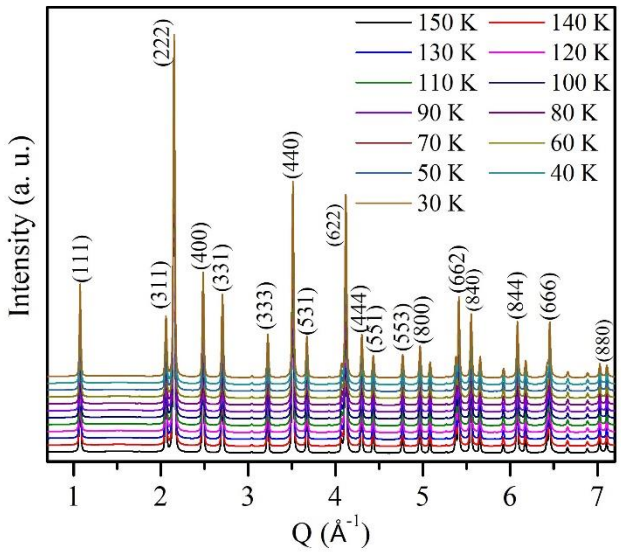

Fig. 7. Synchrotron x-ray diffraction (SRXRD) pattern of polycrystalline $Dy_2Ti_2O_7$ measured at different temperatures.

4.5 Debye-Grüneisen analysis

The temperature-dependent variation of lattice volume has been plotted and shown in Fig. 9. To extract the crystal field induced change in the lattice volume, we fit the data using Debye-Grüneisen equation, accounting the anharmonic parts of lattice vibration due to thermal expansion [33, 34].

$$V \cong V\,(T=0) + \int_0^T \frac{\gamma C_v}{B} dT \cong V\,(T=0) + \frac{9\gamma N k_B}{B} T \left(\frac{T}{\Theta_D}\right)^3 \int_0^{\Theta_D/T} \frac{x^3}{e^x - 1} dx \qquad (1)$$

Where, V(T=0), Θ_D, γ and B represents the volume at 0 K, Debye temperature, the Grüneisen parameters and bulk modulus respectively. V (T=0), Θ_D and $\frac{9\gamma N k_B}{B}$ are the fitting parameters which have been determined by fitting the data in 150 to 70 K temperature range. The obtained values of V (T=0), Θ_D and $\frac{9\gamma N k_B}{B}$ are 1031.92± 0.03Å^3, 337.8± 19.0 K and 0.085± 0.004, respectively. The obtained fitting is extrapolated at low temperature and represented as a solid line in Fig 9. It has been found that the obtained value of Debye temperature is similar to as obtained by Hiroi et al. from specific heat measurement [35]. The fitted temperature-dependent lattice volume shows a clear deviation below ~70 K further confirming the prominence of crystal field at low temperature induces structural distortion in these compounds.

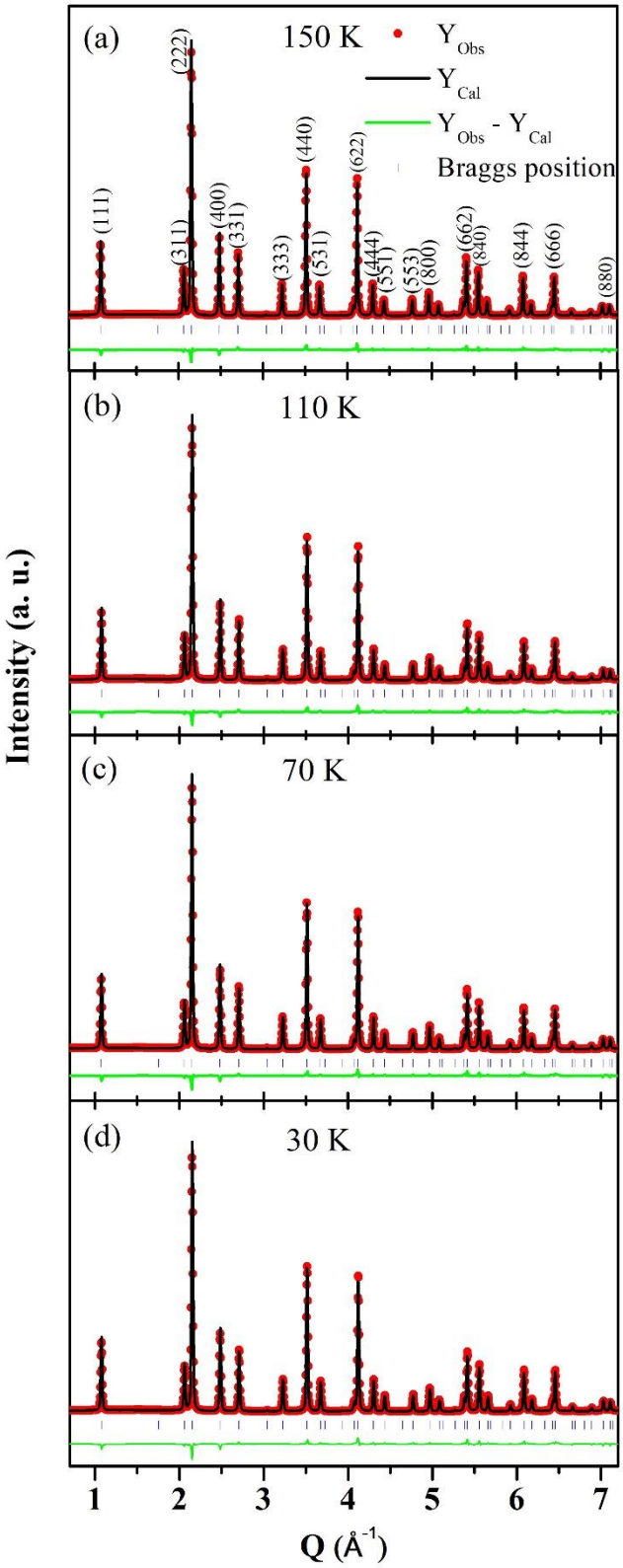

Fig. 8. Rietveld fit of the synchrotron x-ray diffraction pattern measured at 150K, 110 K, 70 K and 30 K for polycrystalline $Dy_2Ti_2O_7$.

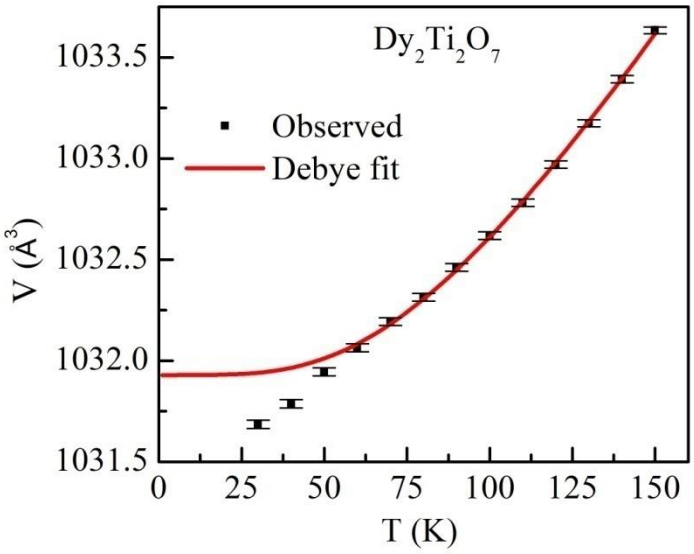

Fig. 9. Temperature-dependent variation of the lattice volume (dot) and modeled Debye – grüneisen fit (solid red line) of $Dy_2Ti_2O_7$.

Table 5. Details of crystallographic parameters and goodness of fit as obtained from Rietveld refinement of low temperature synchrotron x-ray diffraction $Dy_2Ti_2O_7$.

T (K)	A (Å)	*x*	R_p	R_{wp}	R_e	χ^2
150	10.1109(1)	0.3276(1)	4.91	5.24	4.90	1.14
140	10.1101(1)	0.3276(1)	5.07	5.41	4.93	1.20
130	10.1094(1)	0.3276(1)	5.10	5.44	4.94	1.21
120	10.1087(1)	0.3277(0)	5.13	5.46	4.96	1.21
110	10.1081(1)	0.3278(1)	5.19	5.52	4.98	1.23
100	10.1076(1)	0.3278(3)	5.32	5.65	4.99	1.28
90	10.1071(1)	0.3279(1)	5.45	5.76	5.07	1.29
80	10.1066(1)	0.3277(2)	5.46	5.80	4.86	1.42
70	10.1062(1)	0.3276(1)	5.48	5.85	4.71	1.54
60	10.1058(1)	0.3277(3)	5.65	6.04	4.90	1.52
50	10.1054(1)	0.3278(1)	5.77	6.14	4.88	1.58
40	10.1049(1)	0.3279(1)	5.77	6.19	5.00	1.53
30	10.1045(1)	0.3278(1)	5.90	6.30	4.89	1.66

5. Conclusions

Temperature-dependent dielectric measurement shows two distinct relaxations around 90K and 36K in both $Ho_2Ti_2O_7$ and $Dy_2Ti_2O_7$ spin ice compound. Obtained value of critical exponent in Curie-Weiss and Lacroix- *Béné* fitting of relative dielectric permittivity indicates that both relaxations are diffusive and Debye-like in nature. The value of activation energy (E_a), dielectric response and structural analysis of A & B-site doped $Ho_2Ti_2O_7$ shows that both relaxations at 90K and 36K are inherently related to the lattice distortions at O1 (48f) and O2 (8b) sites of structure. The low temperature synchrotron x-ray diffraction studies show that there is no structural phase transition. In these spin ices, crystal field anisotropy splits the multipolar order parameter, which is coupled with structural order parameters. This coupling and pronounced change in crystal electric field splitting of the multipolar order parameter induces structural distortion at O1 and O2 sites of the oxygen position without breaking the crystal symmetries. Low temperature synchrotron x-ray diffraction studies confirm that there are no ferroelectric phase transitions but observed dielectric transitions are thermally activated dielectric relaxations. These results determine the nature and possible cause of the dielectric relaxations prevailing in these spin ice compounds.

Acknowledgment: Authors acknowledge the support of CIFC, IIT (BHU) in collection of high-resolution x-ray diffraction (HRXRD) data. We acknowledge the support from India-DESY project of the Department of Science and Technology, Government of India operated through Jawaharlal Nehru Centre for Advanced Scientific Research, Jakkur, India. We also thank beamline staff of P24at PETRA III, DESY, Hamburg, Germany for their help in setting up the experiments.

Reference

[1] Gardner J. S., Gingras M. J. P., and Greedan J. E., Rev. Mod. Phys. **82**,(2010) 53.

[2] Balents L., Nature **464**, (2010)199.

[3] Ramirez A. P., Hayashi A., Cava R. J., Siddharthan R., and Shastry B. S., Nature **399**,(1999) 333.

[4] Bramwell S. T. and Gingras M. J. P., Science.**294**, (2001)1495.

[5] Siddharthan R., Shastry B., Ramirez A. P., Hayashi A., Cava R. J., and Rosenkranz S., Phys. Rev. Lett. **83**, (1999) 1854.

[6] Rosenkranz S., Ramirez A. P., Hayashi A., Cava R. J., Siddharthan R., and Shastry B.S., J. Appl. Phys. **87**, (2000) 5914.

[7] Rau J. G.and Gingras M. J. P., Phys. Rev. B **92**, (2015) 144417.

[8] Petrenko V. F. and Whitworth R. W., *Physics of Ice* (Clarendon, Oxford, 1999).

[9] Dong X. W., Wang K. F., Luo S. J., Wan J. G., and Liu J. M., J. Appl. Phys. **106**, (2009) 104101.

[10] Lin L., Xie Y. L., Wen J. J., Dong S., Yan Z. B., and Liu J.-M., New J. Phys. **17**, (2015) 123018.

[11] Liu D., Lin L., Liu M. F., Yan Z.B., Dong S., and Liu-J.M., J. Appl. Phys. **113**, (2013) 17D901.

[12] Saito M., Higashinaka R., and Maeno Y., Phys. Rev. B **72**, (2005) 144422.

[13] Mączka M., Sanjuán M. L., Fuentes A. F., Macalik L., Hanuza J., Matsuhira K., and Hiroi Z., Phys. Rev. B **79**, (2009) 214437.

[14] Sergienko I. A. and Curnoe S. H., J. Phys. Soc. Japan **72**, (2003) 1607.

[15] Ruminy M., Chi S., Calder S., and Fennell T., Phys. Rev. B **95**, (2017) 060414.

[16] Ke X., West D. V., Cava R. J., and Schiffer P., Phys. Rev. B **80**, (2009) 144426.

[17] Rodriguez-carvajal J., Phys. B **192**, (1993) 55.

[18] Uchino K. and Nomura S., Ferroelectr. Lett. **44**, (1982) 55.

[19] Bianchi U., Dec J., Kleemann W., and Bednorz J. G., Phys. Rev. B **51**, (1995) 8737.

[20] Nino J. C., Lanagan M. T., Randall C. A., and Kamba S., Appl. Phys. Lett. **81**,(2002) 4404.

[21] Kamba S., Porokhonskyy V., Pashkin A., Bovtun V., Petzelt J., Nino J. C., Trolier-McKinstry S., Lanagan M. T., and Randall C. A., Phys. Rev. B **66**, (2002) 054106.

[22] Cross L.E., Ferroelectrics **151**, (1994) 305.

[23] Lummen T. T. A., Handayani I. P., Donker M. C., Fausti D., Dhalenne G., Berthet P., Revcolevschi A., and Van Loosdrecht P. H. M., Phys. Rev. B **77**, (2008) 214310.

[24] Nakanishi Y., Kumagai T., Yoshizawa M., Matsuhira K., Takagi S., and Hiroi Z., Phys. Rev. B **83**, (2011) 184434.

[25] Bahri Y. and Potter A. C., Phys. Rev. B **92**, (2015) 035131.

[26] Fu L., Phys. Rev. Lett. **115**, (2015) 026401.

[27] Almog A., Bauminger E. R., Levy A., Nowik I., and Ofer S., Solid State Commun. **12**, (1973) 693.
[28] Clancy J. P., Ruff J. P. C., Dunsiger S. R., Zhao Y., Dabkowska H. A., Gardner J. S., Qiu Y., Copley J. R. D., Jenkins T., and Gaulin B. D., Phys. Rev. B **79**,(2009) 014408.
[29] Kitagawa K., Higashinaka R., Ishida K., Maeno Y., Takigawa M., and Dy I., Phys. Rev. B **77**, (2008) 214403.
[30] Ruminy M., Pomjakushina E., Iida K., Kamazawa K., Adroja D. T., Stuhr U., and Fennell T., Phys. Rev. B **94**, (2016) 024430.
[31]Ruminy M., Groitl F., Keller T., and Fennell T., Phys. Rev. B **94**, (2016) 174406.
[32] Blagg R. J., Ungur L., Tuna F., Speak J., Comar P., D. Collison, Wernsdorfer W., McInnes E. J. L., Chibotaru L. F., and Winpenny R. E. P., Nat. Chem. **5**, (2013) 673.
[33] Kiyama T., Yoshimura K., Kosuge K., Ikeda Y., and Bando Y., Phys. Rev. B **54**, (1996) R756.
[34] Yakub E., J. Low Temp. Phys. **187**, (2017) 20.
[35] Hiroi Z., Matsuhira K., Takagi S., Tayama T., and Sakakibara T., J. Phys. Soc. Japan **72**, (2003) 411.